Hybrid Ga_2O_3/AlGaN/GaN Ultraviolet Detector With Gate Metal in the Grooved AlGaN Layer for Obtaining Low Dark Current and Large Detectivity

Zupin Liu, Chunshuang Chu, Bingxiang Wang, Guansen Huang, Ke Jiang, Yonghui Zhang, Xiaojuan Sun, Zi-Hui Zhang, and Dabing Li

***Abstract*— In this work, a metal/Ga_2O_3/AlGaN/GaN hybrid-structured metal–semiconductor–metal ultraviolet photodetector (MSM UV PD) with low dark current has been proposed and fabricated. In the dark condition, the depletion region formed by the metal gate and the AlGaN layer pinches off the two-dimensional electron gas (2DEG) channel, and we can obtain a dark current even lower than 10^{-10} A/cm^2. In the illumination condition, due to the electric field formed by the metal and the Ga_2O_3 layer, the photogenerated electrons will move to the AlGaN/GaN channel to form the 2DEG. We then get a photo-to-dark current ratio of 8.77 $\times$ 10^8. Furthermore, the detectivity of the device is higher than 3.30 $\times$ 10^{12} Jones when a 254-nm UV illumination signal is applied.**

***Index Terms*— Detectivity, metal gate, metal–semiconductor–metal ultraviolet photodetector (MSM UV PD), photo-to-dark current ratio, two-dimensional electron gas (2DEG).**

I. Introduction

ULTRAVIOLET light with the wavelength of 200–280 nm cannot reach the Earth's surface due to the absorption of stratospheric ozone, so it is also called solar-blind ultraviolet (UV) light [1], [2]. Because there is no influence of solar background radiation in the solar-blind range, the solar-blind UV photodetectors (UV PDs) have the advantage of strong anti-interference effect and high detection rate [3], [4]. Based on the above characteristics, solar-blind UV PDs are widely used in UV communication, fire monitoring, and environmental protection [5], [6], [7], [8]. Wide bandgap semiconductor materials, such as AlGaN and Ga_2O_3, are preferred materials for fabricating solar-blind UV PDs. The bandgap of AlGaN can range from 3.4 to 6.2 eV by varying the Al composition [9]. To fabricate AlGaN-based solar-blind UV PDs, the Al composition has to be as high as 0.45. However, the epitaxial growth of AlGaN alloy films with high Al composition and large thickness is a great technical challenge [10], [11]. Ga_2O_3 has natural solar-blind properties with the energy bandgap up to 4.9 eV, which can detect solar-blind UV light [12]. However, at present, there are oxygen vacancies that generate the defect density of 1 $\times$ 10^{16} cm^{-3} in Ga_2O_3 films [13], [14]. High defect density will cause a high dark current that may sacrifice the responsivity and the detectivity [15]. In order to reduce the density of defects, UV–ozone treatment at high temperature can help to reduce the density for oxygen vacancies [16], and by doing so, the dark current level can be decreased. However, another factor influencing the photocurrent and the responsivity is the carrier transport. The electron mobility in the Ga_2O_3 layer is lower than 200 cm^2/V·s because of the scattering effect by defects [17], [18], [19], [20]. Hence, tremendous effort has to be made to improve the crystalline quality for Ga_2O_3 films [14]. Besides that, other attempts to improve the carrier transport efficiency for Ga_2O_3 film are also doable, e.g., graphene-based electrode is utilized for more efficiently collecting the photogenerated carriers, and this helps to increase the response speed and responsivity for Ga_2O_3-based PD [21]. The Schottky contact/Ga_2O_3 interfacial properties can also be engineered by growing an organic material Spiro-MeOTAD layer. The Spiro-MeOTAD modulates the energy band profile between the metal and the Ga_2O_3 layer, which increases the carrier transport and enables a shorter response time [22]. Another approach to increase the carrier transport for Ga_2O_3-based PDs is utilizing a hybrid Ni/Ga_2O_3/GaN heterogeneous structure as our group has reported recently [23]. The Ga_2O_3 layer serves as the optical absorption layer and

Manuscript received 9 July 2022; revised 27 August 2022 and 2 September 2022; accepted 8 September 2022. Date of publication 23 September 2022; date of current version 24 October 2022. This work was supported in part by the National Natural Science Foundation of China under Grant 62074050 and Grant 61725403; in part by the State Key Laboratory of Reliability and Intelligence of Electrical Equipment, Hebei University of Technology under Grant EERI_PI2020008 and Grant EERIPD2021012; in part by the Research Fund by Jiangsu Provincial Key Laboratory of Photonic and Electronic Materials Sciences and Technology, Nanjing University under Grant njuzds2021-005. The review of this article was arranged by Editor J. D. Phillips. *(Zupin Liu and Chunshuang Chu contributed equally to this work.) (Corresponding authors: Zi-Hui Zhang; Dabing Li.)*

Zupin Liu, Chunshuang Chu, Guansen Huang, Yonghui Zhang, and Zi-Hui Zhang are with the State Key Laboratory of Reliability and Intelligence of Electrical Equipment, Tianjin 300401, P. R. China, and also with the Key Laboratory of Electronic Materials and Devices of Tianjin, School of Electronics and Information Engineering, Hebei University of Technology, Tianjin 300401, P. R. China (e-mail: zh.zhang@hebut.edu.cn).

Bingxiang Wang, Ke Jiang, Xiaojuan Sun, and Dabing Li are with the State Key Laboratory of Luminescence and Applications, Changchun Institute of Optics, Fine Mechanics and Physics, Chinese Academy of Sciences, Changchun 130033, China (e-mail: lidb@ciomp.ac.cn).

Color versions of one or more figures in this article are available at https://doi.org/10.1109/TED.2022.3206186.

Digital Object Identifier 10.1109/TED.2022.3206186

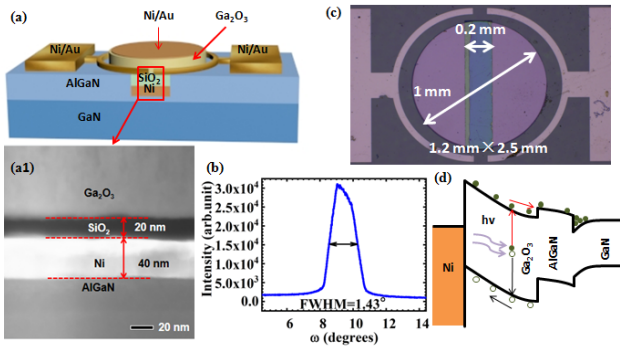

Fig. 1. (a) Schematic for the Ni/Ga_2O_3/AlGaN/GaN UV PD with gate structure. (a1) TEM image for the gate region. (b) High-resolution XRD rocking curve for Ga_2O_3 film. (c) Top view of the fabricated Ni/Ga_2O_3/AlGaN/GaN UV PD. (d) Schematic of the bandgap alignment for the Ni/Ga_2O_3/AlGaN/GaN multiple junctions.

the high-efficiency carrier transport process is favored by the GaN layer. The Ni metal helps to push the photogenerated electrons into the GaN layer. The increased responsivity and the detectivity can also be obtained if one can decrease the dark current.

Hence, in this work, we design a hybrid Ni/Ga_2O_3/AlGaN/GaN structure, in which we have fabricated a gate metal in the grooved AlGaN layer. The advantages of this design include the deep UV light absorption by the Ga_2O_3 layer and the enhanced electron transport in the AlGaN/GaN interface. Note that the AlGaN/GaN interface forms a two-dimensional electron gas (2DEG) channel [24]. In order to reduce the dark current in the AlGaN/GaN structure, we purposely design and fabricate a groove where a Ni-based gate metal is deposited. By doing so, the 2DEG in the AlGaN/GaN channel can be depleted, which helps to decrease the dark current and increase the detectivity for the proposed structure.

II. Experiment

The schematic for the proposed structure is shown in Fig. 1(a). First, we grow a 20-nm-thick GaN buffer layer on a [0001]-oriented sapphire substrate by using a metal-organic chemical vapor deposition (MOCVD) system. Then, a 2-μm-thick unintentionally n-type doped GaN (u-GaN) layer is grown on the buffer layer. Next, we further grow a 70-nm-thick $Al_{0.10}Ga_{0.90}N$ layer on the u-GaN layer. After the epitaxial growth, we use photolithography mask and dry etching process to make a groove in the $Al_{0.10}Ga_{0.90}N$ layer. The groove has a depth of 60 nm and a width of 0.20 mm. Then, a 40-nm-thick Ni gate metal is deposited in the groove by using an electron beam (E-beam) evaporation method, which is followed by a 20-nm-thick SiO_2 layer. The SiO_2 layer is grown by using an atomic layer deposition (ALD) system. Note that we present the cross-sectional TEM image for the gate region in Fig. 1(a1). It can be seen that the thicknesses of the Ni gate metal and the SiO_2 insulation layer are precisely controlled experimentally. After preparing the carrier transport layer, we grow a 400-nm-thick β-Ga_2O_3 layer on top of the AlGaN layer by using another MOCVD system. Fig. 1(b) shows the XRD rocking curve of asymmetric planes for the grown Ga_2O_3 layer. The full-width at half-maximum (FWHM) for the (−201)-planed Ga_2O_3 is 1.43°, which indicates that the grown Ga_2O_3 layer has excellent crystalline quality [25]. After growing the Ga_2O_3 layer, we mask and dry etch the sample to get the Ga_2O_3 mesa. By using an E-beam system, a very thin Ni/Au (5/5 nm) metal stack is deposited on the Ga_2O_3 layer and two Ni/Au (10/10 nm) metal stacks are deposited on the AlGaN layer serving as Schottky contact electrodes. Finally, a 400-nm-thick Au metal is deposited on the two Ni/Au (10/10 nm) Schottky contacts. Fig. 1(c) presents the fabricated device that is taken under the optical microscope. Fig. 1(d) shows the energy band diagram for the proposed device. The photogenerated carriers will be separated after the Ga_2O_3 layer absorbs the light. Then, the electric field formed at the Schottky contact region between Ni and Ga_2O_3 drives the photogenerated electrons toward the $Al_{0.10}Ga_{0.90}N$/GaN interface and forms 2DEG for efficient carrier transport.

The current–voltage characteristics for the fabricated PD are measured by using a Keithley 6487 source meter. The photocurrent is excited by a 254-nm laser on the top side. The spectral responses are measured by utilizing a DSR100 system that is equipped with a xenon lamp, a chopper, a monochromator, a Keithley 6487 source meter, an SR830 lock-in amplifier, and a standard Si detector. All response spectra have been calibrated by using the standard Si detector. The transient response spectra are measured by utilizing a RIGOL DS6104 digital oscilloscope. A pulsed laser with the wavelength of 254 nm is used to measure the photocurrent and transient responses.

III. Results and Discussion

To further investigate the carrier transport processes and the device physics, APSYS software is adopted to calculate the carrier distribution, dark current, photocurrent, and the energy bandgap by solving the continuity equation and Poisson's equation. In our physical models, we set the work function of Ni to 5.15 eV [26]. The mobility for the 2DEG is set as 1980 $cm^2/V{\cdot}s$ [27]. The Shockley–Read–Hall (SRH) recombination lifetime is assumed to be 10 ns [28]. The optical absorption coefficient for Ga_2O_3, AlGaN, and GaN materials in terms of wavelength can be found elsewhere [29], [30]. The wavelength for producing photogenerated carriers is also set to 254 nm.

Fig. 2(a) shows the dark current and the photocurrent for the fabricated device at different biases. It is worth noting that due to the limited measurement scale for our source meter, the precise dark current level cannot be measured. Nevertheless, we can infer that an extremely low dark current smaller than 10^{-10} A/cm^2 can be obtained. When the PD is irradiated by UV light with the intensity of 460 $\mu W/cm^2$, the photocurrent is as high as 10^{-2} A/cm^2 at the applied bias of 10 V, which generates the ratio between photocurrent and dark current larger than 10^8. We believe that the depletion effect by the Ni gate metal reduces the electron density in the $Al_{0.10}Ga_{0.90}N$/GaN channel that allows the device to have such a low dark current. In the illumination condition, the electric field formed by the Ni and Ga_2O_3 layer pushes the photogenerated electrons into the $Al_{0.10}Ga_{0.90}N$/GaN channel and forms 2DEG. The 2DEG enables the device to obtain a high photocurrent.

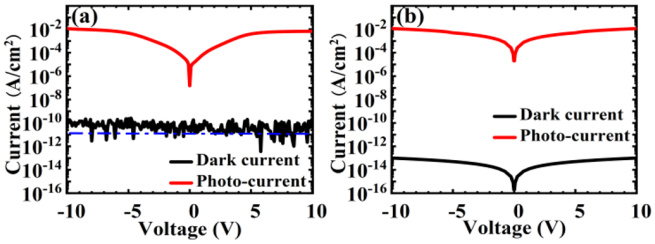

Fig. 2. Dark current and photocurrent density in terms of the applied bias from (a) experimental measurement and (b) numerical calculation. The blue dashed line is the measurement limit for our test system.

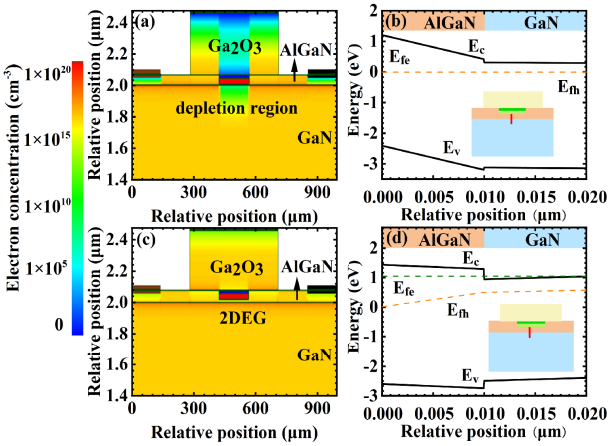

Fig. 3. (a) 2-D profile of the electron concentration for the proposed PD in the case of no UV light illumination. (b) Energy band alignment for AlGaN/GaN region in the case of no UV light illumination. (c) 2-D profile of the electron concentration for the proposed PD in the case of UV light illumination. (d) Energy band alignment for AlGaN/GaN region in the case of UV light illumination. E_c, E_v, E_{fe}, and E_{fh} represent the conduction band, valence band, and quasi-Fermi level for electrons and holes, respectively. The data are calculated at the bias of 0 V.

The numerically calculated results are shown in Fig. 2(b). We notice that the calculated dark current is $\sim 10^{-13}$ A/cm^2. The numerically calculated ratio between the photocurrent and the dark current is 10^{11}, which also evidences the effectiveness of the Ni gate metal in decreasing the dark current and increasing the photocurrent. Note that both experimentally and numerically, the gate Ni metal is not biased.

To further understand the electron concentration in the $Al_{0.10}Ga_{0.90}N$/GaN channel in the dark and light conditions, we calculate and show the 2-D electron concentration profile in the dark condition, as presented in Fig. 3(a). Note that our actual device has a radius of 0.50 mm and a groove width of 0.20 mm. However, because of the limited computer memory, our computation model has scaled down the device size except that the layer thickness and groove depth are the same as the experimentally set values. Fig. 3(a) shows that the Ni gate metal has depleted the electrons in the $Al_{0.10}Ga_{0.90}N$/GaN interface. Fig. 3(b) shows the energy band diagram for the $Al_{0.10}Ga_{0.90}N$/GaN interface under the Ni gate metal region, which also illustrates the absence of the 2DEG at the $Al_{0.10}Ga_{0.90}N$/GaN interface under the Ni gate metal region. As a result, a low dark current is produced. When the device is irradiated with UV light of 254 nm, according to Fig. 3(c), the 2DEG in the $Al_{0.10}Ga_{0.90}N$/GaN interface is retrieved. Fig. 3(d) shows the energy band profile for the $Al_{0.10}Ga_{0.90}N$/GaN interface under the Ni gate metal

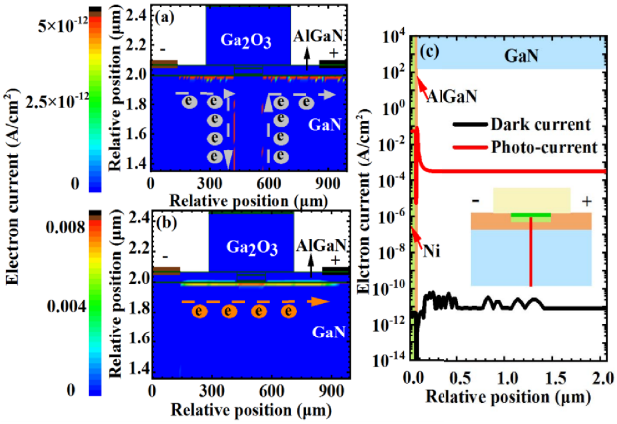

Fig. 4. (a) 2-D profile of the electron current for the proposed PD in the case of no UV light illumination. (b) 2-D profile of the electron current for the proposed PD in the case of UV light illumination. (c) Electron current profiles when the UV light is ON and OFF. The data are calculated at the bias of 4 V.

region, and it demonstrates the generation of 2DEG in the $Al_{0.10}Ga_{0.90}N$/GaN interface. The energy band also indicates that the holes will be stored in the GaN layer, and the electric field in the Ni/Ga_2O_3 junction only pushes the electrons to the GaN layer, while the hole concentration is negligibly low. The 2DEG density at the $Al_{0.10}Ga_{0.90}N$/GaN interface is calculated to be 10^{19} cm^{-3}, which favors the increased photocurrent density.

Next, to further solidify our speculations, we have also computed and shown the electron current flow perpendicular to the [0001] orientation for the proposed PD in dark and UV illumination conditions, respectively. Fig. 4(a) presents the 2-D current profile in the case of no 254-nm light illumination, from which we see an extremely low electron current level at the $Al_{0.10}Ga_{0.90}N$/GaN interface despite the 4-V applied bias. The Ni gate metal in the grooved $Al_{0.10}Ga_{0.90}N$ layer disables the electron current flow. Nevertheless, when the 254-nm light is turned on in our simulation program, the current density at the $Al_{0.10}Ga_{0.90}N$/GaN interface has become significantly increased, as shown in Fig. 4(b). Fig. 4(c) further compares the electron current in the $Al_{0.10}Ga_{0.90}N$/GaN region when the 254-nm light is turned off and turned on. It shows that the electron current is increased by more than 10^8 in magnitude when the 254-nm light is applied. The largest current level occurs at the $Al_{0.10}Ga_{0.90}N$/GaN interface because of the 2DEG formed therein.

Fig. 5(a) shows the measured responsivity as a function of the wavelength for the proposed PD. The responsivity increases as the applied bias on the Schottky contact becomes increased. However, the responsivity is almost unchanged, which is consistent with Fig. 2(a). The saturated current in the proposed PD structure is another proof for the impact of the gate on the pinchoff for the electron channel. We find the responsivity in the wavelength range from 200 to 250 nm, which corresponds to the cutoff absorption edge for the Ga_2O_3 material. An even higher responsivity is obtained when the wavelength exceeds 250 nm, which is believed to be caused by the thick GaN layer. If we define a ratio (R_{350}/R_{250}) between the responsivity at the wavelength of 350 and 250 nm, this value is 3.54 at the applied bias of 2 V. Nevertheless,

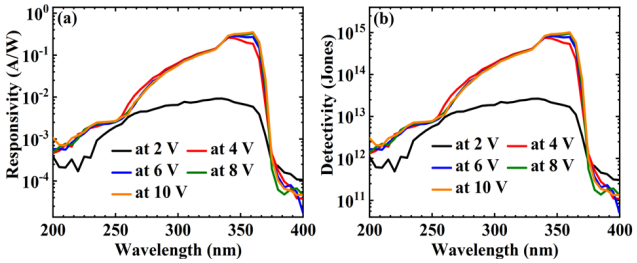

Fig. 5. (a) Spectral responsivity and (b) detectivity in terms of the incident light wavelength at different applied biases.

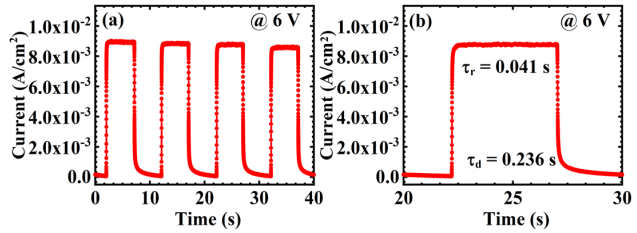

Fig. 6. Time-dependent optical response in (a) multiple cycles and (b) single cycle when a 254-nm UV illumination signal is applied. The applied bias is set to 6 V.

such R_{350}/R_{250} is 18.39 at the applied bias of 2 V in our recent report that utilizes 100-nm-thick Ga_2O_3 layer in the Ga_2O_3/GaN hybrid PD [23]. Hence, the increased Ga_2O_3 layer thickness can more efficiently absorb the deep UV photons. To better address the advantage for our Ga_2O_3/AlGaN/GaN hybrid PD with Ni gate metal, we also calculate the detectivity ($D*$) by using the formula $D^* = R\sqrt{(S/2eI_d)}$, where R is the responsivity in Fig. 5(a), S is the effective illuminated area of 0.00785 cm^2, e is the free electron charge, and I_d is the dark current. Note that, as we have mentioned previously, the dark current in our proposed PD is too low to be tested by our source meter, and hence, we assume I_d to be 1.04×10^{-12} A/cm^2 according to Fig. 2(a). Then, the detectivity at different biases is shown in Fig. 5(b). We compare the dark current and the detectivity in the ~250-nm wavelength for our proposed PD with the values for other reported Ga_2O_3-based UV PDs (see Table I). It shows that our PD shows the lowest dark current level and this is attributed to the electron depletion effect at the $Al_{0.10}Ga_{0.90}N$/GaN interface by the Ni gate metal. It is worth noting that the underestimated dark current can produce the detectivity of 3.30×10^{12} Jones at a low bias of 2 V, and this number can be further increased if a more accurate low dark current can be measured.

Fig. 6(a) shows the photoresponse when multiple optical cycles are used. It can be seen that our device exhibits excellent stability and repeatability because of the $Al_{0.10}Ga_{0.90}N$/GaN 2DEG channel. Besides, Fig. 6(a) shows the time-dependent optical response in a single cycle, from which we can infer a rise time (τ_r) of 0.041 s and a decay time (τ_d) of 0.236 s for the fabricated PD in this work. Note that τ_r is defined as the time interval when the photocurrent increases from 10% to 90% of its peak value and τ_d is defined as the time interval when the photocurrent decreases from 90% to 10% of its peak value [22].

Table I also summarizes and compares the rise time and the decay time for different Ga_2O_3-based PDs. It seems that the rise time for our proposed PD in this work is at a good level,

TABLE I
DETECTIVITY AND RESPONSE TIME FOR THE REPORTED Ga_2O_3-BASED UV PDS IN THE LITERATURE

Material structure	Wavelength (nm)	D* (Jones)	τ_r/τ_d (s)	I_d (A)	Ref
p-Ga_2O_3	250	1.50×10^{15} (5 V)	0.01/0.01 (5 V)	$\sim10^{-10}$ (5 V)	[35]
Au/Ga_2O_3/Au	254	1.77×10^{11} (0 V)	0.03/0.08 (0 V)	1.80×10^{-10} (0 V)	[36]
Graphene/Ga_2O_3	254	2.67×10^{15} (2 V)	-/0.0097 (2 V)	-	[8]
Ga_2O_3/GaN nanowires	254	1.20×10^{11} (10 V)	0.31/0.23 (10 V)	1.60×10^{-10} (10 V)	[37]
Amorphous Ga_2O_3	260	1.70×10^{12} (1 V)	-/-	1.61×10^{-12} (1 V)	[2]
Graphene/Ga_2O_3 /Graphene	254	6.26×10^{11} (5 V)	1.05/0.88 (5 V)	4.06×10^{-9} (5 V)	[7]
GaSe/Ga_2O_3	254	2.52×10^{14} (10 V)	0.00031/ 0.0003 (10 V)	-	[5]
Ni/Ga_2O_3/GaN	254	1.43×10^{14} (10 V)	0.213/0.027 (6 V)	1.90×10^{-11} (10 V)	[23]
Ni/Ga_2O_3/ AlGaN/GaN	254	$>3.30\times10^{12}$ (2 V)	0.041/0.236 (6 V)	$<1.18\times10^{-14}$ (2 V)	this work

and we attribute this to the 2DEG in the $Al_{0.10}Ga_{0.90}N$/GaN channel. We also notice a long decay time for our proposed PD when compared with other structures, which is likely due to the existence of the donor-complex (DX) centers within the AlGaN or GaN epitaxial layers [31]. This is known as the persistence photoconductive (PPC) effect and can be normally observed in PDs with 2DEG [32]. The polarization-induced electric field in the $Al_{0.10}Ga_{0.90}N$/GaN channel can spatially separate the electrons and holes. However, there still exists the Coulomb effect between the 2DEG and the holes in the GaN layer, which attracts the holes in the channel. The traps in the $Al_{0.10}Ga_{0.90}N$/GaN interface may capture the photogenerated holes. When the UV light is switched OFF, such photogenerated holes cannot be quickly released and the depletion region width decreases in the vicinity of Schottky contact that has traps or deep levels. Then, the decay time for the electron current increases. We believe that the PPC effect can be reduced by increasing the temperature of the device such that the holes can get more energy and escape from the traps [33], [34]. Then, the depletion region width in the vicinity of Schottky contact gets increased and the corresponding decay time will subsequently be shortened.

IV. CONCLUSION

In summary, a metal/Ga_2O_3/$Al_{0.10}Ga_{0.90}N$/GaN hybrid-structured MSM UV PD has been proposed and fabricated in this work. The Ni gate metal fabricated in the grooved $Al_{0.10}Ga_{0.90}N$ layer plays an important role in significantly reducing the dark current. The electric field formed by the Ni and Ga_2O_3 layer drives the photogenerated electrons toward the $Al_{0.10}Ga_{0.90}N$/GaN channel and the 2DEG is therefore formed at such heterojunction interface so that an increased

photocurrent can be obtained. We then obtain the decent ratio between photocurrent and dark current that is larger than 10^8. The detectivity in the 254-nm wavelength exceeds 3.30×10^{12} Jones even at the low applied bias of 2 V. Besides, the existence of 2DEG is the key factor for realizing a fast response speed for the demonstrated PD when the UV light is turned on. We believe that the structure proposed in the report contributes to improve the sensitivity and stability of solar-blind UV PDs and the device physics revealed here helps the optoelectronic community to better understand photosensitive devices.

ACKNOWLEDGMENT

The authors would like to thank Beijing MIG Semiconductor Company Ltd. to grow the Ga_2O_3 material.

REFERENCES

[1] D. Kaur and M. Kumar, "A strategic review on gallium oxide based deep-ultraviolet photodetectors: Recent progress and future prospects," *Adv. Opt. Mater.*, vol. 9, no. 9, pp. 1–34, May 2021, doi: 10.1002/adom.202002160.

[2] X. Xiao *et al.*, "Solution-processed amorphous Ga_2O_3:CdO TFT-type deep-UV photodetectors," *Appl. Phys. Lett.*, vol. 116, no. 19, pp. 1–5, May 2020, doi: 10.1063/5.0007617.

[3] Q. Cai *et al.*, "Progress on AlGaN-based solar-blind ultraviolet photodetectors and focal plane arrays," *Light, Sci. Appl.*, vol. 10, no. 1, pp. 1–31, Dec. 2021, doi: 10.1038/s41377-021-00527-4.

[4] K. Li *et al.*, "Solar-blind position-sensitive detectors fabricated from βGa_2O_3/polycrystalline diamond heterojunctions," *Phys. Rapid Res. Ltrs*, vol. 15, no. 10, pp. 1–6, Oct. 2021, doi: 10.1002/pssr.202100347.

[5] Y. Wang *et al.*, "P-GaSe/n-Ga_2O_3 van der Waals heterostructure photodetector at solar-blind wavelengths with ultrahigh responsivity and detectivity," *ACS Photon.*, vol. 8, no. 8, pp. 2256–2264, Aug. 2021, doi: 10.1021/acsphotonics.1c00015.

[6] P.-F. Chi, F.-W. Lin, M.-L. Lee, and J.-K. Sheu, "High-responsivity solar-blind photodetectors formed by Ga_2O_3/p-GaN bipolar heterojunctions," *ACS Photon.*, vol. 9, no. 3, pp. 1002–1007, Mar. 2022, doi: 10.1021/acsphotonics.1c01892.

[7] C. Zeng *et al.*, "Solar-blind ultraviolet detector based on ordered nanoporous βGa_2O_3 film," *Jpn. J. Appl. Phys.*, vol. 61, no. 4, pp. 1–6, Feb. 2022, doi: 10.35848/1347-4065/ac53e4.

[8] P. Tan *et al.*, "Hysteresis-free Ga_2O_3 solar-blind phototransistor modulated from photoconduction to photogating effect," *Appl. Phys. Lett.*, vol. 120, no. 7, pp. 1–7, Feb. 2022, doi: 10.1063/5.0078904.

[9] M. Higashiwaki, R. Kaplar, J. Pernot, and H. Zhao, "Ultrawide bandgap semiconductors," *Appl. Phys. Lett.*, vol. 118, no. 20, pp. 1–4, May 2021, doi: 10.1063/5.0055292.

[10] X. Chen, F. Ren, S. Gu, and J. Ye, "Review of gallium-oxide-based solar-blind ultraviolet photodetectors," *Photon. Res.*, vol. 7, no. 4, pp. 381–415, Apr. 2019, doi: 10.1364/PRJ.7.000381.

[11] J. Y. Tsao *et al.*, "Ultrawide-bandgap semiconductors: Research opportunities and challenges," *Adv. Electron. Mater.*, vol. 4, no. 1, pp. 1–49, Jan. 2018, doi: 10.1002/aelm.201600501.

[12] Y.-S. Zhi *et al.*, "High-responsivity solar-blind photodetector based on MOCVD-grown Si-doped βGa_2O_3 thin film," *Chin. Phys. B*, vol. 30, no. 5, pp. 1–7, May 2021, doi: 10.1088/1674-1056/abe37a.

[13] J. Zhang, J. Shi, D.-C. Qi, L. Chen, and K. H. L. Zhang, "Recent progress on the electronic structure, defect, and doping properties of Ga_2O_3," *APL Mater.*, vol. 8, no. 2, pp. 1–35, Feb. 2020, doi: 10.1063/1.5142999.

[14] X. Hou *et al.*, "Review of polymorphous Ga_2O_3 materials and their solar-blind photodetector applications," *J. Phys. D, Appl. Phys.*, vol. 54, no. 4, pp. 1–35, Jan. 2021, doi: 10.1088/1361-6463/abbb45.

[15] L. Huang *et al.*, "Comparison study of βGa_2O_3 photodetectors grown on sapphire at different oxygen pressures," *IEEE Photon. J.*, vol. 9, no. 4, pp. 1–8, Aug. 2017, doi: 10.1109/JPHOT.2017.2731625.

[16] S. Kim and J. Kim, "Highly selective ozone-treated βGa_2O_3 solar-blind deep-UV photodetectors," *Appl. Phys. Lett.*, vol. 117, no. 26, pp. 1–6, Dec. 2020, doi: 10.1063/5.0030400.

[17] Y. Zhang *et al.*, "MOCVD grown epitaxial βGa_2O_3 thin film with an electron mobility of 176 cm^2/V s at room temperature," *APL Mater.*, vol. 7, no. 2, pp. 1–6, Feb. 2019, doi: 10.1063/1.5058059.

[18] W. Li, K. Nomoto, D. Jena, and H. G. Xing, "Thermionic emission or tunneling? The universal transition electric field for ideal Schottky reverse leakage current: A case study in βGa_2O_3," *Appl. Phys. Lett.*, vol. 117, no. 22, pp. 1–6, Nov. 2020, doi: 10.1063/5.0029348.

[19] Z.-C. Zhang, Y. Wu, C. Lu, and S. Ahmed, "Electron mobility in βGa_2O_3: An ensemble Monte Carlo study," *Appl. Phys. A*, vol. 124, no. 9, pp. 1–5, Sep. 2018, doi: 10.1007/s00339-018-2053-z.

[20] C. Zhang *et al.*, "Electronic transport properties in metal doped beta-Ga_2O_3: A first principles study," *Phys. B, Condens. Matter*, vol. 562, pp. 124–130, Jun. 2019, doi: 10.1016/j.physb.2019.03.004.

[21] M. Chen, J. Ma, P. Li, H. Xu, and Y. Liu, "Zero-biased deep ultraviolet photodetectors based on graphene/cleaved (100) Ga_2O_3 heterojunction," *Opt. Exp.*, vol. 27, no. 6, pp. 8717–8726, Mar. 2019, doi: 10.1364/OE.27.008717.

[22] Z. Yan *et al.*, "High sensitivity and fast response self-powered solar-blind ultraviolet photodetrctor with βGa_2O_3/Spiro-MeOTAD p-n heterojunction," *J. Mater. Chem. C*, vol. 6, no. 5, pp. 972–979, 2018, doi: 10.1039/C7TC03576D.

[23] G. Huang *et al.*, "Hybrid metal/Ga_2O_3 /GaN ultraviolet detector for obtaining low dark current and high responsivity," *Opt. Lett.*, vol. 47, no. 6, pp. 1561–1564, Mar. 2022, doi: 10.1364/OL.454717.

[24] J. Sun *et al.*, "Suspended tungsten trioxide (WO_3) gate AlGaN/GaN heterostructure deep ultraviolet detectors with integrated micro-heater," *Opt. Ex.*, vol. 27, no. 25, pp. 36405–36413, Dec. 2019, doi: 10.1364/OE.27.036405.

[25] A. Kalra, S. Vura, S. Rathkanthiwar, R. Muralidharan, S. Raghavan, and D. N. Nath, "Demonstration of high-responsivity epitaxial βGa_2O_3/GaN metal-heterojunction-metal broadband UV-A/UV-C detector," *Appl. Phys. Exp.*, vol. 11, no. 6, pp. 1–5, Jun. 2018, doi: 10.7567/APEX.11.064101.

[26] S. Arulkumaran, T. Egawa, H. Ishikawa, M. Umeno, and T. Jimbo, "Effects of annealing on Ti, Pd, and Ni/n-$Al_{0.11}Ga_{0.89}N$ Schottky diodes," *IEEE Trans. Electron Devices*, vol. 48, no. 3, pp. 573–580, Mar. 2001.

[27] B. Pandit, E. F. Schubert, and J. Cho, "Dual-functional ultraviolet photodetector with graphene electrodes on AlGaN/GaN heterostructure," *Sci. Rep.*, vol. 10, no. 1, pp. 1–7, Dec. 2020, doi: 10.1038/s41598-020-79135-y.

[28] Z.-H. Zhang *et al.*, "Hole transport manipulation to improve the hole injection for deep ultraviolet light-emitting diodes," *ACS Photon.*, vol. 4, no. 7, pp. 1846–1850, Jul. 2017, doi: 10.1021/acsphotonics.7b00443.

[29] Z. Li *et al.*, "Flexible solar-blind Ga_2O_3 ultraviolet photodetectors with high responsivity and photo-to-dark current ratio," *IEEE Photon. J.*, vol. 11, no. 6, pp. 1–9, Dec. 2019, doi: 10.1109/JPHOT.2019.2946731.

[30] J. F. Muth *et al.*, "Absorption coefficient and refractive index of GaN, AlN and AlGaN alloys," *MRS Internet J. Nitride Semicond. Res.*, vol. 4, no. S1, pp. 502–507, 1999, doi: 10.1557/S1092578300002957.

[31] E. Arslan, S. Bütün, S. B. Lisesivdin, M. Kasap, S. Ozcelik, and E. Ozbay, "The persistent photoconductivity effect in AlGaN/GaN heterostructures grown on sapphire and SiC substrates," *J. Appl. Phys.*, vol. 103, no. 10, pp. 1–7, May 2008, doi: 10.1063/1.2921832.

[32] J. Z. Li, J. Y. Lin, H. X. Jiang, M. A. Khan, and Q. Chen, "Persistent photoconductivity in a two-dimensional electron gas system formed by an AlGaN/GaN heterostructure," *J. Appl. Phys.*, vol. 82, no. 3, pp. 1227–1230, Aug. 1997, doi: 10.1063/1.365893.

[33] X. Tang *et al.*, "Temperature enhanced responsivity and speed in an AlGaN/GaN metal-heterostructure-metal photodetector," *Appl. Phys. Lett.*, vol. 119, no. 1, pp. 1–6, Jul. 2021, doi: 10.1063/5.0054612.

[34] M. Hou, H. So, A. J. Suria, A. S. Yalamarthy, and D. G. Senesky, "Suppression of persistent photoconductivity in AlGaN/GaN ultraviolet photodetectors using *in situ* heating," *IEEE Electron Device Lett.*, vol. 38, no. 1, pp. 56–59, Jan. 2017, doi: 10.1109/LED.2016.2626388.

[35] Z. X. Jiang *et al.*, "P-type β-Ga_2O_3 metal-semiconductor-metal solar-blind photodetectors with extremely high responsivity and gain-bandwidth product," *Mater. Today Phys.*, vol. 14, pp. 1–9, Aug. 2020, doi: 10.1016/j.mtphys.2020.100226.

[36] L. Dong, J. Yu, R. Jia, J. Hu, Y. Zhang, and J. Sun, "Self-powered MSM deep-ultraviolet βGa_2O_3 photodetector realized by an asymmetrical pair of Schottky contacts," *Opt. Mater. Exp.*, vol. 9, no. 3, pp. 1191–1199, Mar. 2019, doi: 10.1364/OME.9.001191.

[37] W. Ding and X. Meng, "High performance solar-blind UV detector based on βGa_2O_3/GaN nanowires heterojunction," *J. Alloys Compounds*, vol. 866, pp. 1–7, Jun. 2021, doi: 10.1016/j.jallcom.2020.157564.